Translational Stroke Research (2019) 10:509–521
https://doi.org/10.1007/s12975-018-0668-1

ORIGINAL ARTICLE

Application of Mesenchymal Stem Cell-Derived Extracellular Vesicles for Stroke: Biodistribution and MicroRNA Study

Gyeong Joon Moon[1,2] · Ji Hee Sung[1,3] · Dong Hee Kim[1,3,4] · Eun Hee Kim[1,3] · Yeon Hee Cho[1,3] · Jeong Pyo Son[1,4] · Jae Min Cha[5] · Oh Young Bang[1,3,4,6]

Received: 9 July 2018 / Revised: 23 September 2018 / Accepted: 2 October 2018 / Published online: 19 October 2018

Abstract

Mesenchymal stem cells (MSCs) exert their therapeutic capability through a variety of bioactive substances, including trophic factors, microRNAs, and extracellular vesicles (EVs) in infarcted tissues. We therefore hypothesized that MSC-derived EVs (MSC-EVs) possess therapeutic molecules similar to MSCs. Moreover, given their nature as nanosized and lipid-shielded particles, the intravenous infusion of MSC-EVs would be advantageous over MSCs as a safer therapeutic approach. In this study, we investigated the biodistribution, therapeutic efficacy, and mode of action of MSC-EVs in a rat stroke model. MSC-EVs successfully stimulated neurogenesis and angiogenesis in vivo. When compared to the MSC-treated group, rats treated with MSC-EVs exhibited greater behavioral improvements than the control group ($p < 0.05$). Our biodistribution study using fluorescence-labeled MSC-EVs and MSCs demonstrated that the amounts of MSC-EVs in the infarcted hemisphere increased in a dose-dependent manner, and were rarely found in the lung and liver. In addition, MSC-EVs were highly inclusive of various proteins and microRNAs (miRNAs) associated with neurogenesis and/or angiogenesis compared to fibro-EVs. We further analyzed those miRNAs and found that miRNA-184 and miRNA-210 were essential for promoting neurogenesis and angiogenesis of MSC-EVs, respectively. MSC-EVs represent an ideal alternative to MSCs for stroke treatment, with similar medicinal capacity but an improved safety profile that overcomes cell-associated limitations in stem cell therapy.

Keywords Stroke · Mesenchymal stem cells · Extracellular vesicles · Neurogenesis · Angiogenesis · MicroRNAs

Introduction

Adult stem cell therapies have been applied to various ischemic diseases, including ischemic heart disease, limb ischemia, and stroke. However, the modest and inconsistent efficacy of adult stem cell therapy has warranted the development of novel clinical strategies [1–3]. In addition, concerns have been raised regarding potential adverse effects of stem cell transplantation in stroke patients, including vascular occlusion by trapping of stem cells in the lung (intravenous applications) or brain vessels (intra-arterial applications) [4, 5]. Recently, it has been suggested that stem cell-derived secretomes or extracellular vesicles (EVs) can be used for stroke therapy as an alternative approach to stem cell infusion methods [3]. In

Electronic supplementary material The online version of this article (https://doi.org/10.1007/s12975-018-0668-1) contains supplementary material, which is available to authorized users.

✉ Oh Young Bang
ohyoung.bang@samsung.com

1 Translational and Stem Cell Research Laboratory on Stroke, School of Medicine, Sungkyunkwan University, Seoul 06351, South Korea

2 School of Life Sciences, BK21 plus KNU Creative BioResearch Group, Kyungpook National University, Daegu 41566, South Korea

3 Stem Cell & Regenerative Medicine Institute for Future Medicine, Samsung Medical Center, Seoul 06351, South Korea

4 Samsung Advanced Institute for Health Sciences and Technology, Sungkyunkwan University, Seoul 06351, South Korea

5 3D Stem Cell Bioprocessing Laboratory, Department of Mechatronics, Incheon National University, Incheon 22012, Republic of Korea

6 Department of Neurology, Samsung Medical Center, School of Medicine, Sungkyunkwan University, Seoul 06351, South Korea

particular, mesenchymal stem cell-derived EVs (MSC-EVs) are known to act as key messengers between MSCs and injured cells, which is one of the major paracrine actions of MSCs [6]. Several preclinical studies have highlighted the pharmacological properties that render MSC-EVs ideal for cell-free therapy targeted toward mediated tissue repair and regeneration of kidney [7], cardiovascular disease [8], and stroke [9]. Thus far, there has been no clinical study examining the effects of MSC-EVs on ischemic diseases, but a phase 1 clinical trial using cord blood-derived MSC-EVs for diabetes patients is currently ongoing (Clinical trial identifier NCT 02138331).

Many studies have documented the therapeutic potential of MSC-EVs for stroke recovery [9–12]; nonetheless, their therapeutic mode of action and biodistribution upon administration in an animal stroke model has not yet been reported. In this study, we conducted various in vivo and in vitro assays using a rat stroke model to evaluate the neurogenic and angiogenic potential and biodistribution of MSC-EVs. In addition, we performed cargo analysis and microRNA (miRNA) studies to verify their therapeutic mode of action in recovery after stroke.

Materials and Methods

Sprague-Dawley (SD) rats were supplied by the Orient Bio Inc. All animal experiments were approved by Institutional Animal Care and Use Committee (IACUC) of Samsung Biomedical Research Institute (SBRI) and performed in accordance with the Institute of Laboratory Animal Resources (ILAR) guide. All animals were maintained in compliance with the relevant laws and institutional guidelines of the Laboratory Animal Research Center (LARC; AAALAC International approved facility) at the Samsung Medical Center.

Cell Culture

Rat bone marrow was obtained from femora and tibias of SD rats (male, 220–250 g, $n = 10–13$). Rat MSCs (rMSCs) were cultured with Dulbecco's modified Eagle's medium (DMEM, Invitrogen, Carlsbad, CA, USA) containing 10% fetal bovine serum, antibiotics, and antifungals (Invitrogen), as previously described [13]. In this study, various primary cell lines were used, including human MSCs [(hMSCs) (Lonza, Basel, Switzerland)], human umbilical endothelial cells [(HUVECs) (ATCC, Manassas, VA, USA)], a fibroblast cell line [(NIH-3T3), (ATCC)], and human neural stem cells [(NSCs) (ReNcell VM, EMD Millipore, Billerica, MA, USA)]. All cells were grown in the recommended media according to the manufacturer's protocol.

Middle Cerebral Artery Occlusion

The transient middle cerebral artery occlusion (tMCAo) was performed using an intraluminal vascular occlusion method, as previously described [14]. Briefly, SD rats (8 weeks old, male, 270–300 g) were anesthetized with 4% isoflurane and maintained with 1.5% isoflurane in 70% N_2O and 30% O_2. Body temperature was maintained at 37.0 to 37.5 °C (measured rectally) with heating pads throughout the surgery and occlusion period. A 4-0 surgical monofilament nylon suture with a rounded tip was advanced from the left common carotid artery into the lumen of the internal carotid artery until it blocked the origin of the middle cerebral artery. Ninety minutes after tMCAo, reperfusion was performed by withdrawing the suture until the tip cleared the lumen of the common carotid artery. Rats with hemorrhagic transformation or subarachnoid hemorrhage caused by rupture of the intracranial artery, as well as rats without observable neurological deficits following MCAo, were excluded from further analyses.

Preparation of Ischemic Brain Tissue Extracts

To obtain ischemic brain tissue extracts (IBE), rats were sacrificed at 3 days after 90 min tMCAo. The ischemic hemispheres were homogenized by adding DMEM (150 mg/mL) on ice. After centrifugation at 10,000×g for 10 min at 4 °C, the supernatants were collected and stored at − 70 °C until use, as previously described [15]. IBE was diluted to 20% with culture media without fetal bovine serum (FBS, Hyclone, Victoria, Australia) and centrifuged at 2500×g for 10 min. The supernatants were centrifuged at 14,000×g for 45 min at 10 °C and filtered with a 0.2-μm bottle top filter (Corning, Inc., Corning, NY, USA) [16].

Isolation of EVs

To stimulate the EV release, MSCs and fibroblast were exposed to 20% IBE, which is considered as the in vitro equivalent to ischemic brain conditions [15–17]. The rMSCs at passage 4 (P4) or fibroblasts were exposed to 20% IBE for 24 h. The conditioned media were centrifuged at 2500×g for 10 min to remove cell debris. The supernatant was transferred to a new tube and centrifuged at 14,000×g for 45 min at 10 °C [18]. The pellets were then resuspended in 20 μL of PBS.

Labeling of MSCs and EVs

rMSCs were resuspended in 100 μL of Neon Resuspension Buffer (Invitrogen) for every two million cells. For electroporation, cells were mixed with 10 μL of the pEGFP-C1 (1.5 μg/μL, Clontech) and aliquoted into a sterile tube. A Neon Tip was inserted into the Neon Pipette and the cell-DNA mixture was aspirated into the tip while avoiding air bubbles. The

Neon Pipette was then inserted into the Neon Tube containing 3 mL of Neon electrolytic buffer E in the Neon Pipette Station. Cells were pulsed once at 1300 V with a width of 40 V. After the pulse, cells were immediately transferred into complete culture media [19]. EVs were labeled with PKH26 or 5-(and-6)-carboxyfluorescein diacetate succinimidyl ester (CFSE; Sigma-Aldrich Corp., St. Louis, USA) for in vivo tracking according to the manufacturer's protocol.

Identification of EVs

To determine the absolute count of EVs, EVs were analyzed using a flow cytometry (FCM) protocol with both side scatter (SSC) and FL1 (488 nm) in logarithmic mode. Nano Fluorescent Size Standard beads (range 220–1330 nm, Spherotech Inc., Lake Forest, IL, USA) were used to set the gate for EV detection. Based on the number of events (N) in the lower right (~ 1.0 μm and green fluorescent protein signal) quadrant of the FCM analysis, the number of EVs was calculated as follows: n/μL = (number of total events / number of bead events) × (assigned bead count / total sample volume). FCM data were acquired on a Calibur flow cytometer using CellQuest software (BD Biosciences, San Jose, CA, USA). Characteristics of EVs (size and morphology) were measured using a Nanosight nanoparticle tracking analysis (NTA, Malvern, UK) and transmission electron microscopy analysis (Hitachi-HT7700, Japan), according to the manufacturer's instructions (Supplemental data).

EV and hMSC Treatment In Vivo

To investigate the effect of rMSC-EVs on neurogenesis and angiogenesis, a total of 113 rats were randomly divided into five groups: sham control group, PBS group, rMSC-EV group, fibro-EV group, and hMSC group. Thirteen rats were included in the sham group. Three animals died within 24 h after tMCAo and were excluded from the study. The rMSC-EVs or fibro-EVs (30 μg/rat) or hMSCs (1×10^6 or 2×10^6 cells/rat) were slowly injected with a 1-mL syringe into the tail vein of the rats 24 h after tMCAo. Three animals without observable neurological deficits were excluded from the PBS group. Two animals with subarachnoid hemorrhage were excluded from both the fibro-EV and hMSC groups. A total of 92 rats were included in the final analysis. For immunostaining and behavioral analysis, 35 rats were divided equally into five groups, and additional animals were allocated to ensure enough animals survived to each time point. Thirty rats were divided into five groups to determine neurogenesis and angiogenesis effects of the different dose of EVs. To analyze the long-term recovery of neurological function, 15 rats were used in cylinder and ladder tests. The experimental timeline is provided in Supplementary Fig. 1.

Behavior Assessments

Behavioral tests were conducted in a blinded fashion for all animals. Modified Neurological Severity Scores (mNSS) were calculated as a measure of motor, sensory, reflex function, and balance using a modified version of sensory tests before tMCAo and 1, 7, and 14 days after tMCAo, as described previously [13]. The cylinder and ladder rung walking tests were performed at 28 days post-injury. For cylinder tests, the animals were placed in a transparent cylinder (diameter 20 cm), and at least 15 contacts of the forelimbs on the wall of the cylinder were recorded for each rat. The number of impaired forelimb contacts was expressed as a percentage of total contacts [20]. A measurement of skilled walking over the ladder was performed using the mean ratio of error per step and presented as a percent of the total [21].

Tissue Preparation

The rats were scarified and transcardially perfused with 4% paraformaldehyde (PFA). The brains were stored in 4% PFA at 4 °C for overnight and then immersed in a 30% sucrose solution for 3–4 days at 4 °C. After fixation and cryoprotection, brains were frozen rapidly in powdered dry ice and stored at − 70 °C. Frozen brains were sectioned coronally between 3 and 4 mm posterior to the bregma to a thickness of 18 μm using a Cryocut Microtome (Leica Microsystems, Germany) and stored in stock solution (0.1 M phosphate buffer pH 7.4, 30% [*v*/*v*] glycerol, 30% ethylene glycol) at 4 °C until use.

Immunostaining

Immunohistostaining was performed as previously described [22]. Samples were fixed with 4% PFA for 1 h and washed with PBS Tween 20 (PBST). Samples were incubated in 0.25% Triton X-100 for 10 min and in 10% horse serum for 1 h. Samples were then incubated overnight at 4 °C with the primary antibody: rabbit anti-Ki67 (diluted 1:500, Abcam, Cambridge, MA, USA), goat anti-doublecortin (anti-DCX, diluted 1:500, Santa Cruz Biotechnology, Santa Cruz, CA, USA), and rabbit anti-von Willebrand factor (anti-vWF, diluted 1:200, Chemicon, Temecula, CA, USA). Samples were then thoroughly washed with PBST, incubated with Dylight-labeled anti-mouse IgG (diluted 1:200, Abcam) or Dylight-labeled anti-rabbit IgG (diluted 1:200, Abcam) for 2 h at room temperature, and washed again with PBST. Samples were mounted with Vectashield mounting medium (Vector Laboratories, Burlingame, CA USA) and imaged via microscopy (EVOS, Advanced Microscopy Group, Mill Creek, WA, USA). The measurements in each block were performed in a blinded fashion. The number of Ki-67/DCX double-positive cells was measured with ImageJ software. The area of vWF was analyzed using Multi Gauge (Fuji Photo Film Co. Ltd., Japan). Data were expressed as the fold change relative to the sham controls.

Western Blots

Western blot analysis was performed as previously described [23]. Proteins were analyzed with rabbit anti-VEGF, c-Met, SDF-1, ephrin A (diluted 1:1000), rabbit anti-GFP antibody (1:2000), and GAPDH (1:5000, Santa Cruz Biotechnology); VEGFR2, HGF, TGF-β, Akt, and phospho-Akt (1:500–1:1000, Cell Signaling Technology, Beverly, MA, USA); CXCR4 and ephrin-A3 (1:1000, Abcam); HSP70, CD63, and flotillin-1 (1: 1000, System Biosciences, Mountain View, CA, USA); and goat anti-Numbl (1:1000, Abcam). The membranes were then incubated with secondary antibodies (Cell Signaling Technology).

MiRNA Analysis

To determine miRNA levels, total RNA was isolated using TRIzol reagent (Gibco-Invitrogen) according to the manufacturer's protocol. RNA (5 μL) was converted to cDNA with a QuantiMir RT System (System Biosciences). Expression levels of miRNAs were analyzed by RT-PCR using a QuantiMir System (System Biosciences). cDNAs were mixed with SYBR®Green Mastermix (Bio-Rad Laboratories, Hercules, CA, USA) and a universal reverse primer. Specific primers (1 μL) were added to each well of the qPCR plate. Expression levels of each mature miRNA were evaluated using the comparative threshold cycle (Ct) method (2−ΔCt). With a cutoff value of 2-fold, changes in the QuantiMir assay were validated with a stem loop-specific reverse-transcription primer and TaqMan PCR Master Mix (Applied Biosystems, Foster City, CA, USA). The level of miRNA was normalized against the level of miR-16 [24, 25].

Transfection of MiRNA

Cells were seeded into 60-mm dishes 24 h before transfection. Transfection experiments were performed using miR-137, miR-184, and miR-210 (Ambion, Austin, TX, USA) and Lipofectamine 2000 (Invitrogen), according to the manufacturer's protocol. A nonspecific miRNA was used as a negative control.

In Vitro Assay

To assess neurogenesis, ReN cells were cultured on a 12-well plate pre-coated with 20 μg/mL laminin (BD Biosciences) with proliferation medium (maintenance medium with 20 ng/mL bFGF and 20 ng/mL EGF) for 2 days. The cells were counted and viability was assessed using trypan blue dye exclusion. A tube formation assay was performed as previously described [26], with some modification. HUVECs were seeded on a Matrigel (BD Biosciences)-coated μ-slide (Ibidi, Fitchburg, WI, USA) in M199 media containing 1% FBS and heparin. The number of loops was quantified using ImageJ software.

Statistical Analysis

In all the experiments, a total of three to six independent experiments were performed to study the neurogenic and angiogenic effects of EVs. Results were expressed as the mean ± standard error of the mean (SEM). Statistical differences between groups were evaluated using a one-way analysis of variance (ANOVA) or two-way ANOVA. Chi-square tests were used to assess the linear trend of the dose-response effect. Statistical analyses were performed using a commercially available software package, SPSS version 23 (SPSS Inc., Chicago, IL, USA). Graphs were drawn using GraphPad Prism 6 (GraphPad Software, La Jolla, CA, USA).

Results

Characterization of EVs

To visualize EVs released from living cells in real time, we employed pEGFP-expressing MSCs, 30–50% of which were GFP positive by 48 h post-transfection (data not shown). We observed the number of subcellular particles considered as EVs that underwent blebbing from plasma membrane of MSCs 6 h after 20% IBE treatment (Fig. 1a, Supplementary Fig. 2 and Supplementary Video). The average size of rMSC-derived EVs showed below 1000 nm, as detected by NTA. NTA analysis showed a size range of 45.5 to 635.5 nm and a concentration range of 3.71×10^9 to 4.46×10^9 per mL of EVs (Fig. 1b). The addition of 1% Triton X-100 caused the complete dissolution of EV structures, indicating that EVs isolated by our protocol were not immune complexes or protein aggregates, but membranous structures of the lipid bilayer [27] (Supplementary Fig. 3). FCM analysis showed that the treatment of MSC cultures with IBE resulted in a significant increase in EV secretion from MSCs compared to the control groups. The EVs in the 20% IBE, which were previously removed by centrifugation and filtration, were much less frequent compared to MSC-EVs (*$p < 0.05$, Fig. 1c, d). We next used TEM to confirm the shapes of EVs from rMSCs and fibroblasts and observed that most EVs had a round or slightly elliptical shape and lacked both a lipid bilayer and nucleus, indicating cell-free conditions (Supplementary Fig. 3).

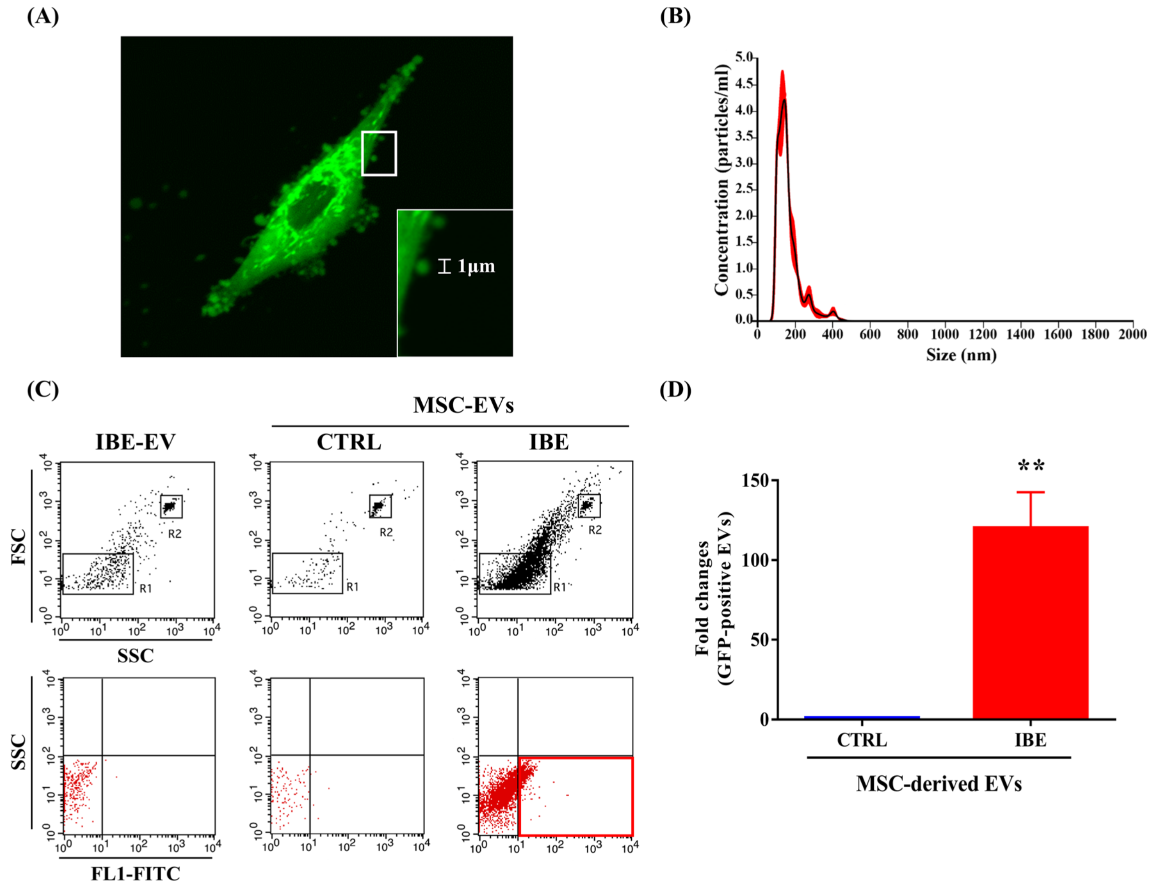

Fig. 1 **a** Fluorescence microscope image of GFP-expressed MSC. EVs are denoted with white box. **b** Representative size distribution profiles of EVs according to NTA analysis. **c** Representative dot plots present GFP intensity versus side scatter intensity for rMSC-EVs counted using 3 μm latex beads as an internal standard. **d** Bar graph representing the number of GFP-positive EVs evaluated by flow cytometry. Data expressed as mean ± SEM (*$p < 0.05$, one-way ANOVA, Tukey post hoc test)

Enhancing Neurogenesis and Angiogenesis In Vivo

To compare neurogenic and angiogenic effects of rMSC-EVs, fibro-EVs, and hMSCs in a rat stroke model, immunohistochemical analysis was performed using Ki-67 (proliferating cells), DCX (immature progenitor neurons), and vWF (angiogenesis) of both ipsilateral and contralateral hemispheres, 14 days after tMCAo. The rats that received rMSC-EVs and hMSCs showed significantly increased co-expression of Ki-67 and DCX in the subventricular zone (SVZ) of both the contralateral and ipsilateral hemispheres (Fig. 2a). The quantitative results, presented as a fold change over the sham control, showed a significant increase in the number of Ki-67/DCX double-positive cells from 7.5- and 5.7-fold (contralateral) and 8.5- and 7.8-fold (ipsilateral) in the SVZ of rMSC-EV-treated and hMSC-treated mice, respectively (Fig. 2b, c; *$p < 0.05$, **$p < 0.01$ vs sham; †$p < 0.05$, ††$p < 0.01$ vs PBS; ‡$p < 0.05$, ‡‡$p < 0.01$ vs fibro-EVs). A significant increase in angiogenesis in the ischemic border zone was also found in rMSC-EV-treated rats (Fig. 2d). When the vWF-positive area in the ischemic boarder zone of the ipsilateral hemisphere was quantified and expressed as a fold change of those in the sham controls, increases of 22.4- and 19.4-fold (contralateral) and 14.2- and 12.5-fold of vWF-positive area were observed in the rMSC-EV-treated and hMSC-treated mice, respectively (Fig. 2e, f; *$p < 0.05$, **$p < 0.01$ vs sham; †$p < 0.05$, ††$p < 0.01$ vs PBS; ‡$p < 0.05$, ‡‡$p < 0.01$ vs fibro-EVs). In general, the neurogenic and angiogenic efficacies of rMSC-EVs were shown to be comparable to those of hMSC-treated groups in our rat stroke model, whereas the PBS- and fibro-EV-treated groups showed significantly lower efficacies. Similarly, a significant increase in both neurogenesis and angiogenesis was observed in rats treated with rMSC-EVs at 28 days post-injury (Supplemental Fig. 4, **$p < 0.01$, *$p < 0.05$ vs PBS).

To clarify whether the neurogenic and angiogenic efficacies of rMSC-EVs are dose dependent, we further examined the effects after administration of PBS and 10, 30, 100, or 300 μg rMSC-EVs in a tMCAo model. We observed a linear trend upon increasing doses of EVs, suggesting that rMSC-EVs promote neurogenesis (chi-square test for linear trend $p < 0.001$) and angiogenesis (chi-square test for linear trend $p < 0.001$) in a dose-dependent manner (Fig. 3).

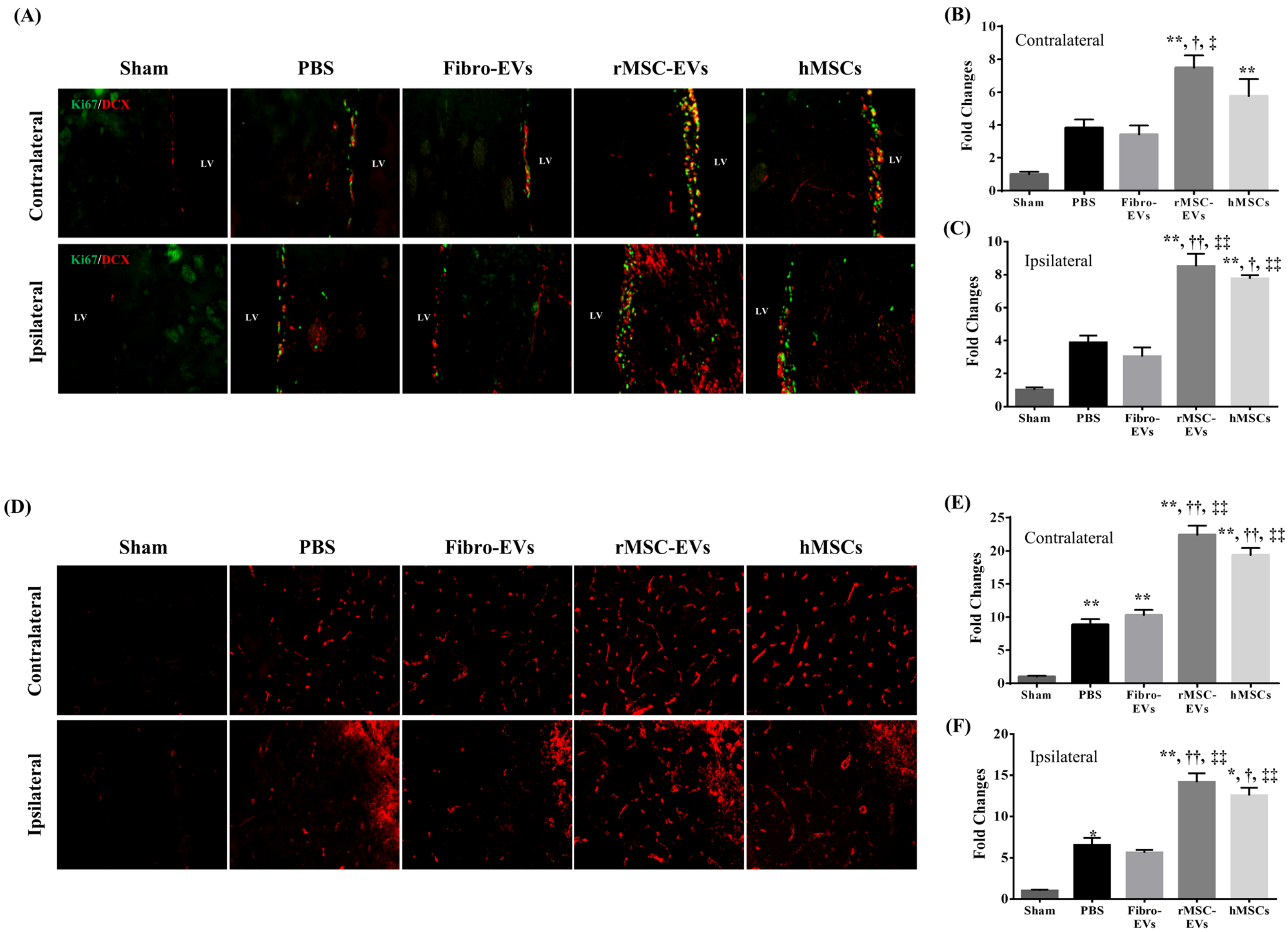

Fig. 2 **a** Representative images of the contralateral and ipsilateral subventricular zone from sham and PBS-, fibro-EV-, rMSC-EV-, and hMSC-treated rats examined for neurogenic effects using DCX immunoreactivity (LV, lateral ventricle). **b**, **c** Bar graph represents the fold changes that were occupied by the number of Ki-67/DCX double-positive cells. **d** Representative images of the striatum immunolabeled for vWF from sham and PBS-, rMSC-EV-, and hMSC-treated rats. **e**, **f** Bar graph represents the fold changes occupied by vWF-positive cells per total field. Data expressed as mean ± SEM ($n = 6$ per group, $*p < 0.05$, $**p < 0.01$ vs sham; $\dagger p < 0.05$, $\dagger\dagger p < 0.01$ vs PBS; $\ddagger p < 0.05$, $\ddagger\ddagger p < 0.01$ vs fibro-EVs; one-way ANOVA, Tukey post hoc test)

Behavioral Recovery Assessments

Mortality rates and behavioral improvements were monitored for 14 days after injection of PBS, fibro-EVs (30 μg/rat), rMSC-EVs (30 μg/rat), or hMSCs (2×10^6 cells/rat). The mortality rate of the rMSC-EV group (5%) was notably lower than that of the other groups: hMSCs (17%), PBS (20%), and fibro-EVs (37%) (Fig. 4a). Neurological function was tested by mNSS scores for 14 days, demonstrating that rMSC-EV treatment significantly improved functional recovery after stroke in the treatment group compared to that of the PBS and fibro-EV groups at 14 days (Fig. 4b, $*p < 0.05$). To evaluate forelimb deficits, we further analyzed the impaired forelimb usage via cylinder and ladder rung walking tests at 28 days post-injury. In 30 μg rMSC-EV-treated rats, an increase in the percent usage of the impaired forelimb was observed as a trend toward significance, compared to the PBS-treated rats (Fig. 4c, $p = 0.09$). In addition, the results of ladder rung walking experiments showed improved skilled walking, although this difference did not reach statistical significance (Fig. 4d). To clarify whether these functional improvements are due to recovery of neuronal fiber bundles (NFBs), we additionally examined the NFB regeneration using diffusion tensor imaging (DTI) based on the 7.0-T animal MRI at 5 weeks after ischemic injury. The DTI results showed that NFBs were significantly increased in the rMSC-EV-treated rats compared to PBS-treated rats (Supplemental Data 5).

Biodistribution of MSC-EVs

rMSC-EVs labeled with CFSE dye were found to migrate into the infarcted brain in our rat stroke model. The CSFE-labeled rMSC-EVs were observed in both ischemic penumbra zone and contralateral hemisphere 3 h post-injection (Fig. 5a). To compare the biodistribution of rMSC-EVs and hMSCs, western blot analysis was performed to measure the accumulation

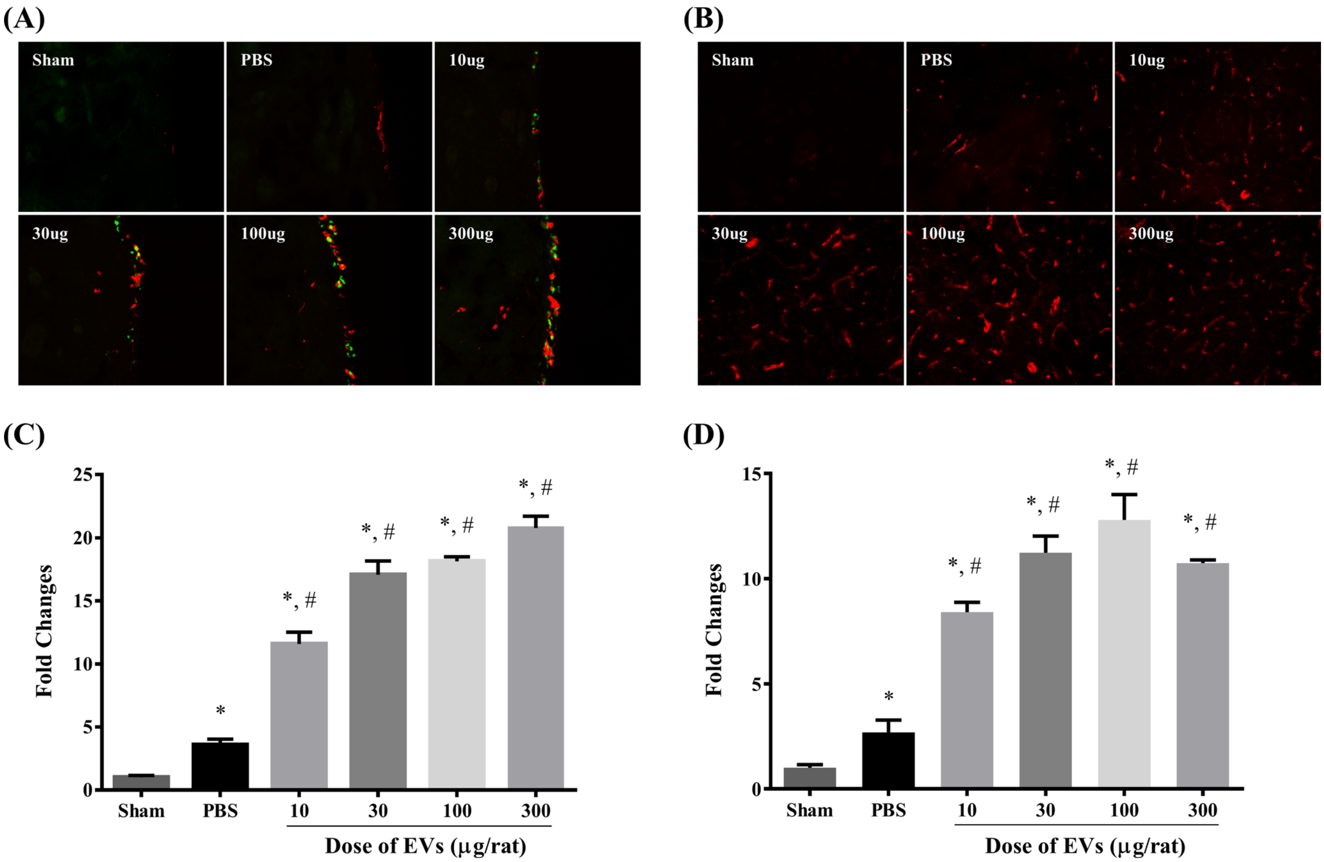

Fig. 3 **a** Double staining of ki-67 (green)/DCX (red) to identify neurogenesis and **b** vWF (red) staining to identify angiogenesis. **c** The number of Ki-67/DCX double-positive cells showed fold changes in the bar graph. **d** The area of vWF positive was counted and described with fold changes in the bar graph. Data expressed as mean ± SEM ($n = 6$ per group, *$p < 0.01$ vs sham, #$p < 0.01$ vs PBS, one-way ANOVA, Tukey post hoc test, chi-square tests were used to assess the linear trend of dose-response effect)

Fig. 4 **a** Kaplan-Meier curve of the survival rate of PBS-, fibro-EV-, rMSC-EV-, and hMSC-treated rats. **b** Neurological deficits were evaluated in PBS-, fibro-EV-, and rMSC-EV-treated groups at 1, 2, 4, 8, and 15 after tMCAo using mNSS. Spontaneous forelimb use being assessed using the cylinder test (**c**) and measurement of skilled walking using ladder rung walking (**d**) at 28 days after tMCAo. Data expressed as mean ± SEM ($n = 7$, *$p < 0.05$ vs PBS, two-way ANOVA for repeated measures, Tukey post hoc test)

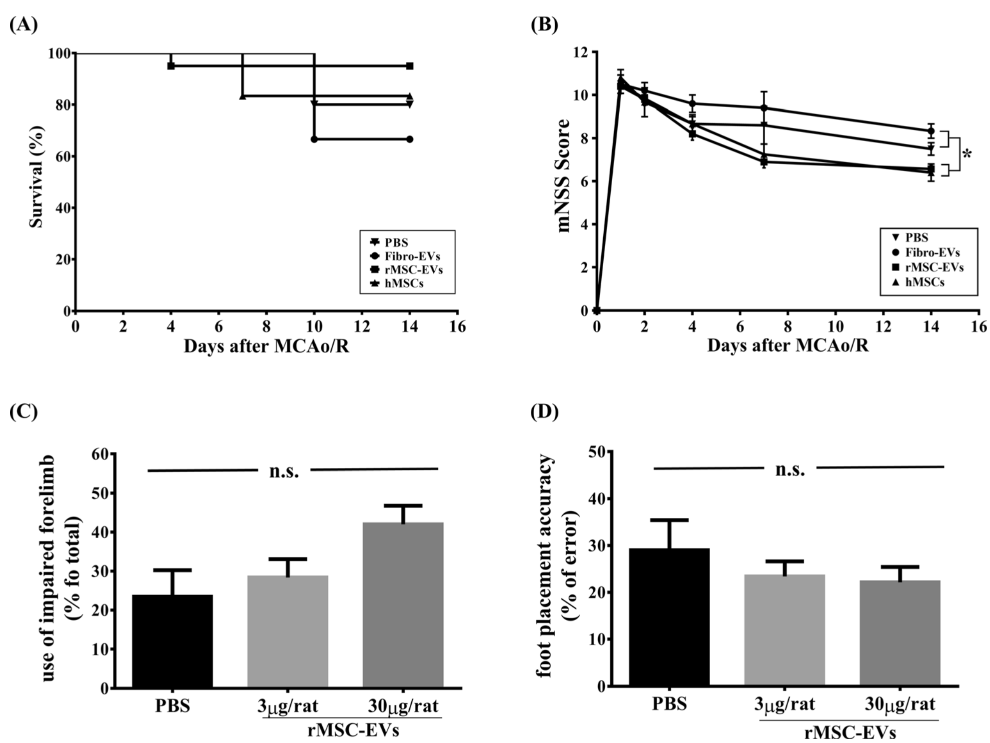

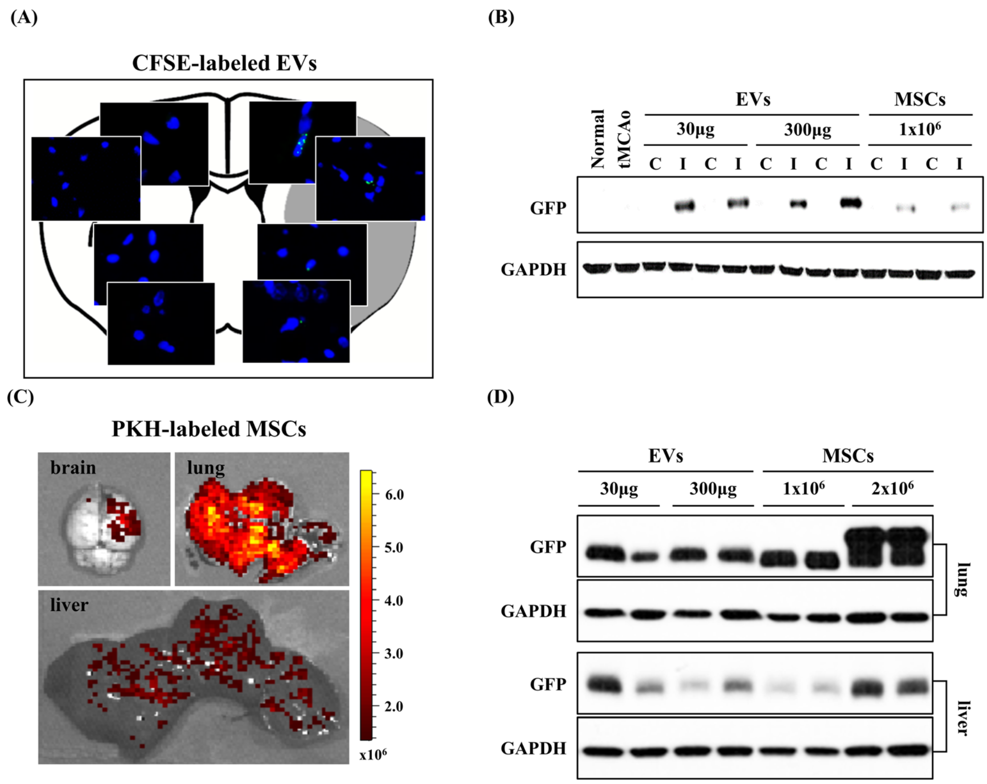

Fig. 5 **a** Representative images of the infarct border zone from CFSE-labeled EV-treated rats (blue: DAPI [4′,6-diamidino-2-phenylindole], green: CFSE). **b** Western blot of brain tissue from normal control, tMCAo only, 30 or 300 μg rMSC-EV-treated, and 1×10^6 rMSC-treated rats examined for EVs in the brain using GFP expression (C, contralateral; I, ipsilateral). **c** Representative images of the brain (upper left), lung (upper right), and liver (below) from 2×10^6 rat MSC-treated rats examined for PKH-labeled MSC tracking using optical ex vivo imaging. **d** GFP expression in the lung and liver was determined by western blot analysis ($n = 6$)

of GFP in the brain, lung, and liver. The rMSC-EV group showed higher levels of GFP in the infarcted brain than the hMSC group (Fig. 5b). On the other hand, considerably larger amounts of hMSCs were trapped within the lung after injection (Fig. 5c, d). Notably, rMSC-EVs accumulated in the infarcted hemisphere in a dose-dependent manner (30–300 μg), but not in the lung and liver. In contrast, hMSCs accumulated more in the lung and liver by increasing the injection doses from 1×10^6 to 2×10^6 cells.

Investigation of EV Cargos: Proteins and miRNAs

We next analyzed the composition of rMSC-EVs that were collected from IBE-treated rMSC cultures. Western blot analysis determined that our rMSC-EVs contained various cargo proteins associated with angiogenesis, neurogenesis, and cell survival. Compared with fibro-EVs, VEGF, VEGFR2, HGF, c-Met, CXCR4, and phospho-Akt (pAkt) were highly presented in the rMSC-EVs. HSP70 and flotillin-1, as extracellular vesicle markers, were detected in both fibro-EVs and rMSC-EVs (Fig. 6a).

We also verified the microRNA inclusions in rMSC-EVs using selected 42 miRNAs known to play a role in neurogenesis and angiogenesis. Semiquantitative analysis showed that miRNA expression patterns differed between rMSC-EVs and fibro-EVs (data not shown). Among the 42 miRNAs, miR-320, miR-296, miR-210, miR-184, miR-155, miR-137, and miR-134 were confirmed to be more abundant in rMSC-EVs than in fibro-EVs (2-fold cutoff threshold), as determined using a TaqMan PCR assay (Fig. 6b).

Neurogenesis and Angiogenesis Mediated by MSC-EVs and MiRNAs

Among the miRNAs that were most abundant in our MSC-EVs, miR-137, miR-184, and miR-210 were known to be major players to stimulate neurogenesis and angiogenesis. Thus, we verified whether these miRNAs were key neurogenic and angiogenic factors included in rMSC-EVs. To investigate the respective effects of individual miR-137, miR-184, and miR-210, their miRNA precursors (pre-miR) were transfected into ReN cells and HUVECs. Random sequences of pre-miR were used as control sequences. In the proliferation analysis of neuronal stem cells, transfection of miR-184 led to increased proliferation of ReN cells, which was comparable to rMSC-EV (Fig. 7a, $^{**}p < 0.01$). The expression of endogenous Numbl was also investigated as a downstream target of miR-184. Our western blot analysis demonstrated that the Numbl expression in ReN cells was significantly decreased by both miR-184 and rMSC-EV compared to the control (Fig. 7c, $^{**}p < 0.01$).

Next, to examine the capability of miR-210 and rMSC-EVs for vascular tube formation, a tubular formation assay was conducted in HUVECs plated on Matrigel, and the resulting loop numbers were counted. The highest efficacy of HUVEC tube formation resulted from rMSC-EVs, while miR-210 also

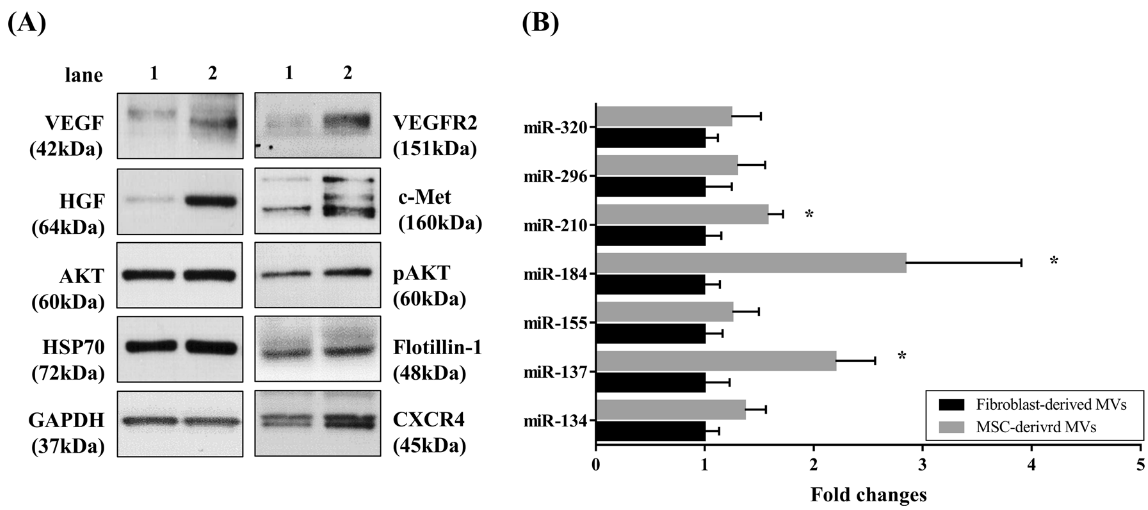

Fig. 6 **a** Protein levels within EVs determined by western blot analysis (lane 1: fibro-EVs, lane 2: rMSC-EVs). **b** Fold changes of miRNA expression within EVs between fibro-EVs and rMSCs-EVs ($n = 5$ per group, $*p < 0.05$, independent sample t test)

induced a significant increase compared to the control (Fig. 7b, $**p < 0.01$). To investigate the downstream target underlying miR-210 regulation in HUVECs, the expression of endogenous ephrin-A3 (EFNA3) was analyzed via western blot. We observed that EFNA3 expression in HUVEC was significantly decreased by both MSC-EV and miR-210 compared to the control (Fig. 7d, $**p < 0.01$). Notably, miR-137 had no effect on neurogenesis and angiogenesis (Supplementary Fig. 6).

Discussion

The main findings of this study are as follows: (1) MSCs release EVs in response to the ischemic brain microenvironment; (2) intravenously injected MSC-EVs, as well as MSCs, promoted neurogenesis and angiogenesis in a dose-dependent manner to support recovery after stroke; (3) MSC-EVs can effectively migrate into the infarcted brain, avoiding cell trapping in the lung and liver; and (4) miRNAs such as miR-184 and miR-210 contained in MSC-EVs may be associated with the therapeutic efficacy for neurogenesis and angiogenesis, respectively.

MSCs secrete a variety of soluble bioactive substances, such as cytokines, trophic factors, and stem cell factors [28, 29]. Our study suggested that MSC-EVs could serve as an effective alternative therapeutic agent to live MSCs, in particular for neurologic improvement after stroke. The data presented in this study were consistent with those of recent studies by other groups [9, 10, 30]. For example, it was reported that intravenous administration of EVs derived from MSCs promoted neurogenesis, functional recovery, and suppression of delayed immune response after ischemic stroke.

In previous reports, animal models of ischemic injury in the heart and brain showed that MSC transplantation resulted in a degree of protective effects in the defected organs although MSCs were not detected in the ischemic regions [31, 32]. These results would support the possibility that MSCs trapped in undesired organs release EVs to the circulatory system homing to the ischemic regions and eventually contributing to therapeutic processes. We have previously reported that the number of circulating MSC-EVs increases in patients with stroke [16]. Other perspectives would suggest that MSCs may migrate into the injured brain after transplantation [33]. However, injected MSCs in the infarcted brain existed only for 1–3 days after transplantation although maximal behavioral improvement was observed after 7–14 days. These results also support the importance of EVs in that transplanted MSCs could communicate with cells in the infarcted tissues and release EVs which might remain and influence the recovery after stroke. In this study, we stimulated the EV release from MSCs by IBE treatment to biochemically mimic the ischemic brain microenvironment. Thus, we could successfully obtain a large amount of MSC-EVs with a variety of neurogenic and angiogenic factors. Our results demonstrate that unlike MSCs, MSC-EVs could migrate into the infarcted brain and directly promote neurogenesis and angiogenesis with improved safety profiles compared to MSCs.

The precise mechanism of the therapeutic action of EVs remains unclear. EVs contain various bioactive substances, including membrane proteins, cytoplasmic proteins, mRNAs, and microRNAs, and deliver them to recipient cells. A previous study suggested that the main mechanism for the therapeutic effects of EVs might be through the transfer of miRNAs to the diseased cells [34]. There were also recent studies reporting that miRNAs were involved in the recovery process after stroke [35], and miRNAs in MSC-EVs influenced the physiology and pathophysiology microenvironments in stroke models [10], as well as cardiac regeneration and protection [36]. Our data also supported the important role of miRNAs such as miR-184 and miR-210 largely contained

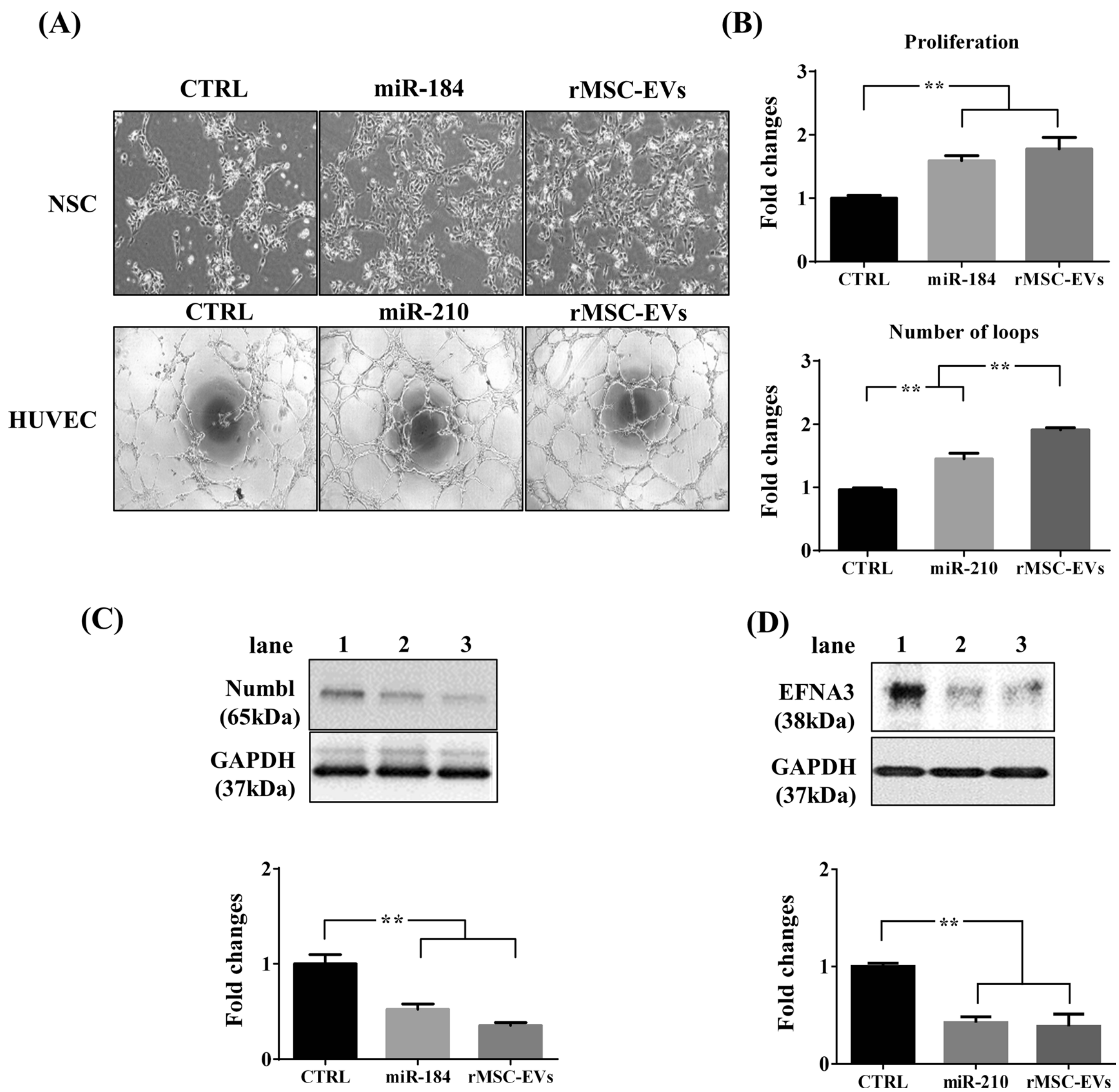

Fig. 7 **a** miR-184 modulates the proliferation of ReN cells. Representative images of ReN cells after treated with rMSC-EVs, transfected with miR-184 or control-miR (left). Quantitative data is shown with fold changes in bar graphs (right). **b** miR-210 induces the tubing formation of HUVEC. Representative images of HUVEC after treated with rMSC-EVs, transfected with miR-210 or control-miR (left). Quantitative data is shown with fold changes in bar graphs (right). **c** Western blot analysis of Numbl in ReN cells (upper). Quantitative data of Numbl level were scaled to relevant GAPDH (below). **d** Western blot analysis of ephrin-A3 in HUVEC (upper). Quantitative data of HUVEC level were scaled to relevant GAPDH (below). Data expressed as mean ± SEM ($n = 3$ per group, $^{**}p < 0.01$, one-way ANOVA, Tukey post hoc test)

in MSC-EVs for neurogenesis and angiogenesis, respectively. Previous reports demonstrated that miR-184 promoted the proliferation of NSCs and inhibited differentiation by repressing Numbl [37]. Moreover, miR-210 played a role in HUVEC migration, as well as tubular differentiation, depending on HIF-1α signaling through repression of EFNA3 [38, 39]. In this study, the analysis of correspondent miRNAs in MSC-EVs and their target downstream signals was consistent with those of previous findings.

One of the major problems with systemic administration of stem cells is cell trapping within organs responsible for bloodstream filtration (first-pass effect). Preclinical studies showed that less than 1% of transplanted cells remained in the target tissue and most of them were found in the liver, spleen, and lung [40]. Moreover, cases of severe pulmonary embolism after intravenous application of MSCs have been reported in both animals and humans [41, 42]. To avoid the first-pass effect and improve the sustainability of MSCs in the diseased site, the intra-arterial injection approach was attempted to bypass pulmonary circulation. However, this route may cause arterial occlusion resulting in stroke, and its efficacy was revealed to be lower than the intravenous injection approach for recovery after stroke [4, 43]. Our present study demonstrated that systemically introduced MSC-EVs migrated into the brain, especially to the infarcted hemisphere. The precise mechanisms of migration of these EVs are unknown, but our results (Fig. 5) led us to speculate that MSC-EVs express chemokine receptors such as CXCR4 (a CXC chemokine receptor) that would facilitate targeting to the ischemic regions, as previously reported [16]. Furthermore, in contrast to MSCs, MSC-EVs were relatively smaller in size and can therefore more easily cross the blood-brain barrier and reach the ischemic regions in the brain while circulating in the bloodstream-protected membranous structures of the phospholipid bilayer [44].

Although our study would contribute to a better understanding of the therapeutic actions of MSC-EVs in stroke models, critical hurdles to translate MSC-EVs to clinical therapeutics still remain. IBE used in this study successfully stimulated EV secretions of MSCs that contained various neurogenic and angiogenic factors. However, this approach using IBE for MSC-EV production would not be suitable for clinical application. Therefore, further studies designed with clinically applicable methods are needed. For example, EV release from cells could be stimulated by various chemically and/or mechanically adapted microenvironments [45, 46]. Moreover, the inclusions in EVs could be controlled by different culture conditions [47, 48]. In our future studies, such preliminary work will be implemented and amended to scale up MSC-EV productions with customized therapeutic properties. A standardized protocol for quality control involving MSC-EV should be conceived for successful clinical application and may include (1) a desirable EV isolation method from culture media, (2) a normalized characterization of the physical properties of EVs, and (3) stringent analysis of the cargo proteins and miRNAs in EVs.

Lastly, although the recent guidelines for animal research were followed (Supplementary Table 1) [49], female animals and animals with stroke risk factors were not used in the present study because we focused on the biodistribution and mechanisms of action of EVs. Further studies using animal models to incorporate stroke risk factors are needed.

In conclusion, this study demonstrated that MSC-EVs could be modulated by biochemically adapted microenvironments. Furthermore, their mode of therapeutic action and clinical feasibility for effective recovery after stroke were proven by our results from various in vivo and in vitro analyses. Our study suggests that MSC-EVs would be an ideal alternative to MSCs to treat stroke patients, while possessing the equivalent or possibly higher therapeutic capacity with better safety profiles compared to current MSC infusion therapy.

Authors' Contributions G.J.M.: conception and design, manuscript writing, financial support, collection and/or assembly of data, data analysis and interpretation, administrative support, final approval of manuscript; J.H.S.: provision of study material, collection and/or assembly of data, data analysis and interpretation; D.H.K.: collection and/or assembly of data, data analysis and interpretation, provision of study material; E.H.K.: collection and/or assembly of data, data analysis and interpretation, provision of study material; Y.H.C.: collection and/or assembly of data, data analysis and interpretation, provision of study material; J.P.S.: collection and/or assembly of data, data analysis and interpretation, provision of study material; J.M.C.: collection and/or assembly of data, provision of study material; O.Y.B.: conception and design, financial support, final approval of manuscript.

Funding This study was supported by a grant from the Korean Healthcare Technology R&D Project, Ministry of Health & Welfare (HI14C1439, HI14C3484, HI17C1256) and Basic Science Research Program, the Ministry of Science, ICT and Future Planning (NRF-2013R1A1A2058139 and NRF-2014R1A1A1004645).

Compliance with Ethical Standards

Conflict of Interest The authors declare that they have no conflicts of interest.

Ethical Approval All animal experiments were approved by the Institutional Animal Care and Use Committee (IACUC) of Samsung Biomedical Research Institute (SBRI, Approval No. 20140203001) and performed in accordance with the Institute of Laboratory Animal Resources (ILAR) guide. All animals were maintained in compliance with the relevant laws and institutional guidelines of the Laboratory Animal Research Center (LARC; AAALAC International approved facility, No. 001003) at the Samsung Medical Center.

References

1. Gyongyosi M, Wojakowski W, Lemarchand P, Lunde K, Tendera M, Bartunek J, et al. Meta-analysis of cell-based CaRdiac stUdiEs (ACCRUE) in patients with acute myocardial infarction based on individual patient data. Circ Res. 2015;116(8):1346–60. https://doi.org/10.1161/CIRCRESAHA.116.304346.
2. Peeters Weem SM, Teraa M, de Borst GJ, Verhaar MC, Moll FL. Bone marrow derived cell therapy in critical limb ischemia: a meta-analysis of randomized placebo controlled trials. Eur J Vasc Endovasc Surg. 2015;50(6):775–83. https://doi.org/10.1016/j.ejvs.2015.08.018.
3. Bang OY, Kim EH, Cha JM, Moon GJ. Adult stem cell therapy for stroke: challenges and progress. J Stroke. 2016;18(3):256–66. https://doi.org/10.5853/jos.2016.01263.
4. Pendharkar AV, Chua JY, Andres RH, Wang N, Gaeta X, Wang H, et al. Biodistribution of neural stem cells after intravascular therapy for hypoxic-ischemia. Stroke. 2010;41(9):2064–70. https://doi.org/10.1161/STROKEAHA.109.575993.
5. Chen J, Li Y, Wang L, Zhang Z, Lu D, Lu M, et al. Therapeutic benefit of intravenous administration of bone marrow stromal cells after cerebral ischemia in rats. Stroke. 2001;32(4):1005–11.
6. Tetta C, Ghigo E, Silengo L, Deregibus MC, Camussi G. Extracellular vesicles as an emerging mechanism of cell-to-cell communication. Endocrine. 2013;44(1):11–9. https://doi.org/10.1007/s12020-012-9839-0.
7. Gatti S, Bruno S, Deregibus MC, Sordi A, Cantaluppi V, Tetta C, et al. Microvesicles derived from human adult mesenchymal stem cells protect against ischaemia-reperfusion-induced acute and chronic kidney injury. Nephrol Dial Transplant. 2011;26(5):1474–83. https://doi.org/10.1093/ndt/gfr015.
8. Bian S, Zhang L, Duan L, Wang X, Min Y, Yu H. Extracellular vesicles derived from human bone marrow mesenchymal stem cells promote angiogenesis in a rat myocardial infarction model. J Mol

Med (Berl). 2014;92(4):387–97. https://doi.org/10.1007/s00109-013-1110-5.
9. Xin H, Li Y, Cui Y, Yang JJ, Zhang ZG, Chopp M. Systemic administration of exosomes released from mesenchymal stromal cells promote functional recovery and neurovascular plasticity after stroke in rats. J Cereb Blood Flow Metab. 2013;33(11):1711–5. https://doi.org/10.1038/jcbfm.2013.152.
10. Xin H, Li Y, Liu Z, Wang X, Shang X, Cui Y, et al. MiR-133b promotes neural plasticity and functional recovery after treatment of stroke with multipotent mesenchymal stromal cells in rats via transfer of exosome-enriched extracellular particles. Stem Cells. 2013;31(12):2737–46. https://doi.org/10.1002/stem.1409.
11. Ophelders DR, Wolfs TG, Jellema RK, Zwanenburg A, Andriessen P, Delhaas T, et al. Mesenchymal stromal cell-derived extracellular vesicles protect the fetal brain after hypoxia-ischemia. Stem Cells Transl Med. 2016;5(6):754–63. https://doi.org/10.5966/sctm.2015-0197.
12. Li Y, Cheng Q, Hu G, Deng T, Wang Q, Zhou J, et al. Extracellular vesicles in mesenchymal stromal cells: a novel therapeutic strategy for stroke. Exp Ther Med. 2018;15(5):4067–79. https://doi.org/10.3892/etm.2018.5993.
13. Li WY, Choi YJ, Lee PH, Huh K, Kang YM, Kim HS, et al. Mesenchymal stem cells for ischemic stroke: changes in effects after ex vivo culturing. Cell Transplant. 2008;17(9):1045–59.
14. Moon GJ, Cho YH, Kim DH, Sung JH, Son JP, Kim S, et al. Serum-mediated activation of bone marrow-derived mesenchymal stem cells in ischemic stroke patients: a novel preconditioning method. Cell Transplant. 2018;27(3):485–500. https://doi.org/10.1177/0963689718755404.
15. Choi YJ, Li WY, Moon GJ, Lee PH, Ahn YH, Lee G, et al. Enhancing trophic support of mesenchymal stem cells by ex vivo treatment with trophic factors. J Neurol Sci. 2010;298(1–2):28–34. https://doi.org/10.1016/j.jns.2010.09.003.
16. Kim SJ, Moon GJ, Cho YH, Kang HY, Hyung NK, Kim D, et al. Circulating mesenchymal stem cells microparticles in patients with cerebrovascular disease. PLoS One. 2012;7(5):e37036. https://doi.org/10.1371/journal.pone.0037036.
17. Bang OY, Moon GJ, Kim DH, Lee JH, Kim S, Son JP, et al. Stroke induces mesenchymal stem cell migration to infarcted brain areas via CXCR4 and C-Met signaling. Transl Stroke Res. 2017;8:449–60. https://doi.org/10.1007/s12975-017-0538-2.
18. Turola E, Furlan R, Bianco F, Matteoli M, Verderio C. Microglial microvesicle secretion and intercellular signaling. Front Physiol. 2012;3:149. https://doi.org/10.3389/fphys.2012.00149.
19. Moore JC, Atze K, Yeung PL, Toro-Ramos AJ, Camarillo C, Thompson K, et al. Efficient, high-throughput transfection of human embryonic stem cells. Stem Cell Res Ther. 2010;1(3):23. https://doi.org/10.1186/scrt23.
20. Schallert T, Fleming SM, Leasure JL, Tillerson JL, Bland ST. CNS plasticity and assessment of forelimb sensorimotor outcome in unilateral rat models of stroke, cortical ablation, parkinsonism and spinal cord injury. Neuropharmacology. 2000;39(5):777–87.
21. Metz GA, Whishaw IQ. Cortical and subcortical lesions impair skilled walking in the ladder rung walking test: a new task to evaluate fore- and hindlimb stepping, placing, and co-ordination. J Neurosci Methods. 2002;115(2):169–79.
22. Kim DH, Seo YK, Thambi T, Moon GJ, Son JP, Li G, et al. Enhancing neurogenesis and angiogenesis with target delivery of stromal cell derived factor-1alpha using a dual ionic pH-sensitive copolymer. Biomaterials. 2015;61:115–25. https://doi.org/10.1016/j.biomaterials.2015.05.025.
23. Moon GJ, Shin DH, Im DS, Bang OY, Nam HS, Lee JH, et al. Identification of oxidized serum albumin in the cerebrospinal fluid of ischaemic stroke patients. Eur J Neurol. 2011;18(9):1151–8. https://doi.org/10.1111/j.1468-1331.2011.03357.x.
24. Schwarzenbach H, da Silva AM, Calin G, Pantel K. Data normalization strategies for microRNA quantification. Clin Chem. 2015;61(11):1333–42. https://doi.org/10.1373/clinchem.2015.239459.
25. Qi P, Cheng SQ, Wang H, Li N, Chen YF, Gao CF. Serum microRNAs as biomarkers for hepatocellular carcinoma in Chinese patients with chronic hepatitis B virus infection. PLoS One. 2011;6(12):e28486. https://doi.org/10.1371/journal.pone.0028486.
26. Cha JM, Shin EK, Sung JH, Moon GJ, Kim EH, Cho YH, et al. Efficient scalable production of therapeutic microvesicles derived from human mesenchymal stem cells. Sci Rep. 2018;8(1):1171. https://doi.org/10.1038/s41598-018-19211-6.
27. Gyorgy B, Modos K, Pallinger E, Paloczi K, Pasztoi M, Misjak P, et al. Detection and isolation of cell-derived microparticles are compromised by protein complexes resulting from shared biophysical parameters. Blood. 2011;117(4):e39–48. https://doi.org/10.1182/blood-2010-09-307595.
28. Chen X, Li Y, Wang L, Katakowski M, Zhang L, Chen J, et al. Ischemic rat brain extracts induce human marrow stromal cell growth factor production. Neuropathology. 2002;22(4):275–9.
29. Majumdar MK, Thiede MA, Mosca JD, Moorman M, Gerson SL. Phenotypic and functional comparison of cultures of marrow-derived mesenchymal stem cells (MSCs) and stromal cells. J Cell Physiol. 1998;176(1):57–66. https://doi.org/10.1002/(SICI)1097-4652(199807)176:1<57::AID-JCP7>3.0.CO;2-7.
30. Doeppner TR, Herz J, Gorgens A, Schlechter J, Ludwig AK, Radtke S, et al. Extracellular vesicles improve post-stroke neuroregeneration and prevent postischemic immunosuppression. Stem Cells Transl Med. 2015;4(10):1131–43. https://doi.org/10.5966/sctm.2015-0078.
31. Preda MB, Ronningen T, Burlacu A, Simionescu M, Moskaug JO, Valen G. Remote transplantation of mesenchymal stem cells protects the heart against ischemia-reperfusion injury. Stem Cells. 2014;32:2123–34. https://doi.org/10.1002/stem.1687.
32. Borlongan CV, Hadman M, Sanberg CD, Sanberg PR. Central nervous system entry of peripherally injected umbilical cord blood cells is not required for neuroprotection in stroke. Stroke. 2004;35(10):2385–9. https://doi.org/10.1161/01.STR.0000141680.49960.d7.
33. Rosenblum S, Wang N, Smith TN, Pendharkar AV, Chua JY, Birk H, et al. Timing of intra-arterial neural stem cell transplantation after hypoxia-ischemia influences cell engraftment, survival, and differentiation. Stroke. 2012;43(6):1624–31. https://doi.org/10.1161/STROKEAHA.111.637884.
34. Gyorgy B, Szabo TG, Pasztoi M, Pal Z, Misjak P, Aradi B, et al. Membrane vesicles, current state-of-the-art: emerging role of extracellular vesicles. Cell Mol Life Sci. 2011;68(16):2667–88. https://doi.org/10.1007/s00018-011-0689-3.
35. Xin H, Li Y, Chopp M. Exosomes/miRNAs as mediating cell-based therapy of stroke. Front Cell Neurosci. 2014;8:377. https://doi.org/10.3389/fncel.2014.00377.
36. Nouraee N, Mowla SJ. miRNA therapeutics in cardiovascular diseases: promises and problems. Front Genet. 2015;6:232. https://doi.org/10.3389/fgene.2015.00232.
37. Liu C, Teng ZQ, Santistevan NJ, Szulwach KE, Guo W, Jin P, et al. Epigenetic regulation of miR-184 by MBD1 governs neural stem cell proliferation and differentiation. Cell Stem Cell. 2010;6(5):433–44. https://doi.org/10.1016/j.stem.2010.02.017.
38. Fasanaro P, D'Alessandra Y, Di Stefano V, Melchionna R, Romani S, Pompilio G, et al. MicroRNA-210 modulates endothelial cell response to hypoxia and inhibits the receptor tyrosine kinase ligand Ephrin-A3. J Biol Chem. 2008;283(23):15878–83. https://doi.org/10.1074/jbc.M800731200.
39. Pulkkinen K, Malm T, Turunen M, Koistinaho J, Yla-Herttuala S. Hypoxia induces microRNA miR-210 in vitro and in vivo ephrin-A3 and neuronal pentraxin 1 are potentially regulated by miR-210.

FEBS Lett. 2008;582(16):2397–401. https://doi.org/10.1016/j.febslet.2008.05.048.
40. Phinney DG, Prockop DJ. Concise review: mesenchymal stem/multipotent stromal cells: the state of transdifferentiation and modes of tissue repair—current views. Stem Cells. 2007;25(11):2896–902. https://doi.org/10.1634/stemcells.2007-0637.
41. Jung JW, Kwon M, Choi JC, Shin JW, Park IW, Choi BW, et al. Familial occurrence of pulmonary embolism after intravenous, adipose tissue-derived stem cell therapy. Yonsei Med J. 2013;54(5):1293–6. https://doi.org/10.3349/ymj.2013.54.5.1293.
42. Tatsumi K, Ohashi K, Matsubara Y, Kohori A, Ohno T, Kakidachi H, et al. Tissue factor triggers procoagulation in transplanted mesenchymal stem cells leading to thromboembolism. Biochem Biophys Res Commun. 2013;431(2):203–9. https://doi.org/10.1016/j.bbrc.2012.12.134.
43. Yang B, Migliati E, Parsha K, Schaar K, Xi X, Aronowski J, et al. Intra-arterial delivery is not superior to intravenous delivery of autologous bone marrow mononuclear cells in acute ischemic stroke. Stroke. 2013;44(12):3463–72. https://doi.org/10.1161/STROKEAHA.111.000821.
44. Simpson RJ, Jensen SS, Lim JW. Proteomic profiling of exosomes: current perspectives. Proteomics. 2008;8(19):4083–99. https://doi.org/10.1002/pmic.200800109.
45. Liu ML, Scalia R, Mehta JL, Williams KJ. Cholesterol-induced membrane microvesicles as novel carriers of damage-associated molecular patterns: mechanisms of formation, action, and detoxification. Arterioscler Thromb Vasc Biol. 2012;32(9):2113–21. https://doi.org/10.1161/ATVBAHA.112.255471.
46. Zhang HC, Liu XB, Huang S, Bi XY, Wang HX, Xie LX, et al. Microvesicles derived from human umbilical cord mesenchymal stem cells stimulated by hypoxia promote angiogenesis both in vitro and in vivo. Stem Cells Dev. 2012;21(18):3289–97. https://doi.org/10.1089/scd.2012.0095.
47. Cocucci E, Racchetti G, Meldolesi J. Shedding microvesicles: artefacts no more. Trends Cell Biol. 2009;19(2):43–51. https://doi.org/10.1016/j.tcb.2008.11.003.
48. Ratajczak MZ, Kucia M, Jadczyk T, Greco NJ, Wojakowski W, Tendera M, et al. Pivotal role of paracrine effects in stem cell therapies in regenerative medicine: can we translate stem cell-secreted paracrine factors and microvesicles into better therapeutic strategies? Leukemia. 2012;26(6):1166–73. https://doi.org/10.1038/leu.2011.389.
49. Vahidy F, Schabitz WR, Fisher M, Aronowski J. Reporting standards for preclinical studies of stroke therapy. Stroke. 2016;47(10):2435–8. https://doi.org/10.1161/STROKEAHA.116.013643.